

# Positron annihilation studies on N<sup>+</sup> implantation induced vacancy type defects and its recovery in SI: 6H- SiC

K. Kamalakkannan <sup>a</sup>, C. Lakshmanan <sup>b</sup>, R. Rajaraman <sup>b</sup>, B. Sundaravel <sup>b</sup>, G. Amarendra <sup>b</sup>, K. Sivaji <sup>a,\*</sup>

<sup>a</sup> Department of Nuclear Physics, University of Madras, Guindy Campus, Chennai 600025, India

<sup>b</sup> Materials Science Group, Indira Gandhi Centre for Atomic Research, HBNI, Kalpakkam 603102, India



## ARTICLE INFO

**Keywords:**  
Ion implantation  
Positron annihilation spectroscopy  
Defects  
SI- 6H-SiC

## ABSTRACT

Variable energy positron beam with Doppler broadening spectroscopy (DBS) was used to investigate the depth-resolved defects formed by two fluencies of 130 keV N<sup>+</sup> implanted in Semi Insulating (SI) 6H-SiC. The implanted ions induced damages near the surface and to a depth of 300 nm as simulated by SRIM analysis. Defects recovery, accumulation, and its behavior with two annealing temperatures were also considered. Defect types and its effect on annealing were analyzed from the changes in electron momentum and modeled as layers using variable energy positron fitting (VEPFIT) methods. Inclusion of electric field strength in the fitting procedure supported layer characteristics and the state of charge carriers. Di-vacancies, vacancy complexes observed in the damaged layers were agglomerated at the surface and tend to cure on annealing.

## 1. Introduction

Silicon carbide (SiC), a most promising wide band gap semiconductor is widely in use and progress for high power, high-frequency device applications due to high saturated electron drift velocity, high mobility, and extreme hardness [1–5]. SiC is also a promising semiconductor for spintronics and photonics due to the spin coherence property of some of its lattice defects [6,7] and a promising substrate in GaN-based blue LED devices in optoelectronics applications [8]. For many potential applications and to improve the performance, controlled dopant levels need to be introduced to make p- and/or n-type as well as insulating layers. Controlled high-density selective depth doping by conventional thermal diffusion process for multilayered structures is much involved and limited in dense materials due to dopants saturation at high temperature [9–14]. Fabrication of layer structures including the device isolation layer is more ease in semi-insulating (SI) SiC materials [15,16]. Commercially available SI- SiC is much considered for many applications to have low parasitic capacitance and resistance and also for the improved performance of microwave and field-effect transistor [16,17]. Selective depth doping by ion implantation techniques with controlled ion energy and flux for high-density n/p type layer formation can be realized with the highest precision and patterning [9,11]. However, ion implantation alters the material properties due to predominant

ion collisions with atoms through electronic and nuclear energy loss mechanism. Resulting in the process, various redundant defects with bond breakages lead to amorphization that alters the mechanical strength, electrical and thermal conductivity [18,19]. Kimoto et al. reported the severity of damage in 30, 80, and 140 keV N<sup>+</sup> implantation in p-type 6H- SiC [11]. Also, irradiation-induced effects of rapid amorphization were reported for 50 keV N<sup>+</sup> implantation at 80 K for 4° off-axis orientated 6H- SiC [14,20]. H<sup>+</sup> implantation in 6H- SiC also showed a significant defect formation with structure changes due to the formation of most probable open volume defects such as vacancies, vacancy clusters, ion-vacancy complexes, voids, and antisites [19,21,22]. Vacancy complexes (V<sub>Si</sub>-N<sub>C</sub>) were also identified as a useful defect like a qubit for quantum computing applications [19,23,24]. Identification of defects and their type by qualitative characterization methods at the atomic level and their quantification is very much essential to tune for the device-related properties as well as for advanced applications.

Many analytical methods were explored to describe the defects and structural changes owing to ion implantation [25–27]. Interaction and evolution of these defects created by implantation in semiconductors can be characterized using techniques like electron spin resonance spectroscopy (ESR), deep level transient spectroscopy (DLTS), infrared absorption spectroscopy (IRAS), Rutherford backscattering (RBS), Raman and Positron annihilation spectroscopy (PAS). ESR explores the

\* Corresponding author.

E-mail address: [sivaji@unom.ac.in](mailto:sivaji@unom.ac.in) (K. Sivaji).

charged defects associated with unpaired electrons and DLTS probes defects which result in deep energy levels. Defects that are IR active, like di-vacancies can be successfully probed with IRAS provided with significant concentration. RBS is very effective in probing the displaced atoms as a result of implantation and hence provides information about interstitial defects. Raman spectroscopy is also a conventional characteristic technique for the identification of the defects through vibrations from deformation [28]. Among all, PAS is a powerful technique to identify the implantation induced defects at the atomic level that gives qualitative and quantitative information on the type and concentrations of depth-resolved defects [18,27,29]. In particular, variable energy positron beam coupled with Doppler broadening spectroscopy (DBS) is widely used to deduce the depth-resolved information on open volume defects even at a very low concentration deduced from the annihilation of an electron–positron pair [30–32]. Variable energy positron fitting (VEPFIT) and modelling procedures have been well used to extract defect-related parameters from the measurement of variable energy positron beam coupled DBS technique. The fitting procedures with many models for layered structures effectively identify the implantation induced defects such as mono vacancies ( $V_{Si}$ ,  $V_C$ ), di-vacancies ( $V_{Si}V_C$ ,  $V_CV_C$ ), ion-vacancy complex ( $V_{Si}-N_C$ ), antisites ( $V_CV_{Si}$ ), and vacancy clusters (larger voids, open volumes, and agglomeration of defects) in the ion-implanted SiC [19,33,34]. Linez et al. [19] have reported the possible six types of vacancy defects in 6H-SiC from the DBS measurements and correlated with positron lifetime measurements. Barthe et al. [33] reported the agglomeration of defects into larger voids induced by proton implantation ( $E = \sim 180$  keV) and its annealing behaviour in 6H-SiC. Gentis et al. [35] studied the production of two types of di-vacancies at the surface in Au<sup>+</sup> irradiated ( $E = 20$  MeV) in 6H-SiC at different dose rates. Brauer et al. [36] have also reported the vacancy agglomeration in the near-surface with moderate annealing of Ge<sup>+</sup> implanted 6H-SiC ( $E = 200$  keV) at a fluence range from  $10^{14}/cm^2$  to  $10^{15}/cm^2$ . Further, Yu et al. [37] discussed the agglomeration of defects upon 800 °C to 1400 °C annealing on 800 keV Ge<sup>+</sup> implanted 4H-SiC with a dose rate of  $2 \times 10^{16}/cm^2$ . Hai Yun Wang et al. [38] and Kawasuso et al. [39] have studied the deep centers and defect migration towards the surface upon annealing in the electron irradiated 6H-SiC. Brauer et al. [10] reported the 120 keV N<sup>+</sup> implantation induced vacancy type defects and its agglomeration in the near-surface upon annealing and also for N<sup>+/Al<sup>+</sup> over Al<sup>+/N<sup>+</sup> co-implanted 6H-SiC. Though many studies were reported on the defect dynamics of N<sup>+</sup> implantation in SiC, it is not well explored in semi-insulating 6H-SiC types at low energy ion implantation. Considering the technological importance of creating selective depth high dense N layer in SI- 6H-SiC using low energy implantation with different fluencies are conducted. Also, presenting the nature of defects, defects accumulation from near-surface to the implanted region, and its recovery mechanism probed using variable energy positron beam coupled DBS measurements.</sup></sup>

## 2. Experimental

Monte Carlo simulation of stopping and range of ions in matter (SRIM- 2013) analysis [40] was used to optimize and understand the effect of 130 keV Nitrogen (N<sup>+</sup>) implantation with a specific dose at depth in SiC. Based on the analysis and required layer thickness, low energy N<sup>+</sup> implantation was performed using an in-house low energy gaseous ion implanter at Materials Science Group, IGCAR, Kalpakkam, India. Commercial grade Semi insulating (SI) 6H-SiC (0001) wafer (350 μm thick) was diced to  $1 \times 1 cm^2$  for implantation and positron DBS measurements. The samples were appropriately surface cleaned with acetone, ethanol, and rinsed with double distilled water to remove any contaminated surface stains. The samples mounted in a ladder were at room temperature and the implantation was done sequentially with an energy of 130 keV with fluencies ( $\phi$ )  $10^{15}N^+/cm^2$  and  $10^{16}N^+/cm^2$  under  $1 \times 10^{-6}$  mbar pressure such that the rasterized ion beam impinges the plane oriented to (0001) [27,28]. The implantation time

depends on the dose and the available beam current. The implanted samples are named SCN15 and SCN16 for  $10^{15}N^+/cm^2$  and  $10^{16}N^+/cm^2$ , respectively.

A variable energy beam (0–25 keV) setup coupled with Doppler broadening spectroscopy (DBS) at Materials Science Group, IGCAR, India was used for depth-resolved measurements [27,41,42]. The positron energy can be varied from 0.2 keV to 22 keV with a step size of 0.5 keV by a beam voltage controller in the positron beam accelerator. Slow Positrons (derived from a 50 mCi Na-22 source) emerging after the Tungsten moderator gets into a specific depth of the sample. The mean depth of the implanted positron can be calculated from the relation [43–45].

$\langle z \rangle = \frac{AE^n}{\rho}$  (nm) (1) where,  $A$  is constant (i.e.,  $40 \times 10^{-6} g/cm^2$  keV<sup>-1.7</sup>),  $n = 1.7$  and  $\rho = 3.22 g/cm^3$  (density of SiC). The positron depth profile, P(x), with the specific implantation energy can be derived from the Makhovian profile relation [46],

$$P(x) = \frac{2x}{x_o^2} \exp \left[ - \left( \frac{x}{x_o} \right)^2 \right] \quad (2)$$

where,  $x_o = 1.13 \langle z \rangle$ , and  $x$  the positron implantation depth in nm. After thermalization and diffusion ( $\sim 100$  nm) two annihilated gamma quanta emerges with a broadening ( $511 \text{ keV} \pm \Delta E$ ) from the site of localization. The annihilation characteristics at the sight of positrons depend on the electron density variation at defect sites. Also, the motion of the positrons is dependent on the electric field strength, if any, present inside the samples [47,48]. The relation of electron momentum ( $P_\perp$ ), energy broadening ( $\Delta E$ ) and light velocity ( $c$ ) is given as,

$$\Delta E = \frac{P_\perp c}{2} \quad (3)$$

The energy broadening was measured with a single HPGe detector (having 30% efficiency and energy resolution of 1.27 keV – at 662 keV of Cs-137) mounted normal to the sample kept under  $1 \times 10^{-6}$  mbar pressure. The change denoted as S-parameter reflect the effect of annihilation with valence electrons in the low momentum region ( $511 \pm 1$  keV). Accumulated momentum spectrum to a sum of  $10^6$  counts for each span of positron energy for pristine (SCP), SCN15, and SCN16 samples was collected by a 4 K-MCA. The linear combination of fractions (f) of positron annihilation in the defect and bulk (b) can be defined as,

$$S(E) = f_{surface}(E)S_{surface} - f_{bulk}(E)S_{bulk} + \sum_i f_i(E)S_i \quad (4)$$

where i denotes the defect type [31].

VEPFIT code is widely used to extract accurate values for the S-parameter from various layers as shown in equation (4), and the positron annihilation fraction in these layers. This is based on the solution of the time-averaged positron diffusion equation in any material including materials having electric field. The time-averaged positron density c(z) at a particular depth (z) below the solid surface can be written as [45],

$$D^+ \frac{d^2 c}{dz^2} - \frac{d}{dz} (v_d c) + I(z) - k_t n_t c - \lambda_b c = 0 \quad (5)$$

where,  $c(z)$  = time-averaged positron density,  $v_d$  = drift velocity,  $I(z)$  = positron stopping rate at depth z,  $n_t$  = defect density,  $k_t$  = rate constant for positron trapping at defects,  $\lambda_b$  = bulk annihilation rate,  $D^+$  = positron diffusion coefficient.

By introducing normalized positron stopping profile and boundary conditions, the defect parameters such as diffusion length, constant S parameter, and boundary width for i<sup>th</sup> layer can be extracted. To study the defects in various layers, the initial input parameters such as S value, boundary width, diffusion length, and electric field are used with different VEPFIT fitting models. Among them, model 5 is widely used for a layered structure which allows choosing the free choice of all the input parameters. Further, the implantation induced internal electric field also

play a crucial role in the drifting of low energy positron towards the surface [48]. The electric field contribution was also included in the VEPFIT to obtain an effective fit in high dose samples. For 6H-SiC parameters of  $\langle m \rangle = 2.13$ ,  $n = 1.77$  and  $A = 2.36 \mu\text{g cm}^{-2} \text{keV}^{-n}$  was used [43]. DBS measurements were repeated for SCN15A8, SCN16A8 (annealed SCN15, SCN16 at 800 °C for 30 min in vacuum under  $1 \times 10^{-6}$  mbar) and for SCN15A10, SCN16A10 (annealed SCN15A8, SCN16A8 at 1000 °C for 30 min in vacuum under  $1 \times 10^{-6}$  mbar) samples.

### 3. Results and discussions

SRIM analyzed implantation depth, the relative number of vacancies, and the 6 keV positrons Makhovian stopping profile is shown in Fig. 1. The profile indicates a total ion range for 130 keV with an atomic concentration increase from surface to  $\sim 200$  nm and decreased up to  $\sim 300$  nm. The profile indicates the number of vacancies  $V_{\text{Si}}$  and  $V_{\text{C}}$  in the host lattice, centered at  $\sim 179$  nm with the ion distribution at  $\sim 200 \pm 50$  nm straggling. Defects with various sizes are probable due to the dominant electronic stopping in the surface and nuclear stopping at the ion range maximum. The vacancy distribution for Si and C shows a significant increase of damage from the surface to a maximum within the ion distribution range. The Si-vacancy concentration is predominantly higher than the C-vacancy. The calculated ion density of  $10^{19}\text{N}^+/\text{cm}^3$  and  $10^{20}\text{N}^+/\text{cm}^3$  indicated the experimental dose selection of  $1 \times 10^{15}\text{N}^+/\text{cm}^2$  and  $1 \times 10^{16}\text{N}^+/\text{cm}^2$ . To analyze the damage regions the vacancy distribution profile was considered as different regions from the surface to ion depth.

Figure 2 displays the S-parameter vs. positron energy (mapped with the mean implantation depth) for the pristine (SCP), as-implanted (SCN15 and SCN16) along with depth-dependent S-values. The pristine S-values exponentially decreases from surface to a depth of 1.0 μm and as constant up to 1.5 μm. For SCN15 and SCN16, the S-parameter increases up to  $\sim 70$  nm and decreases steadily closer to the pristine indicate the presence of vacancy type defects at different depths. A significant increase of S-value is seen in SCN16 than in SCN15 and pristine, indicates the increase of vacancy type defects owing to higher damage. These defects are the potential positron trap centers that are attributed to the formation of a higher concentration of open volume defects. Increased S-value beyond 300 nm in as-implanted samples is due to the positron diffusion of about 200 nm. Also, the Gaussian profile depicted in Fig. 1 for 6 keV positron energy shows the annihilation from the surface and beyond the ion range maximum [32,49].

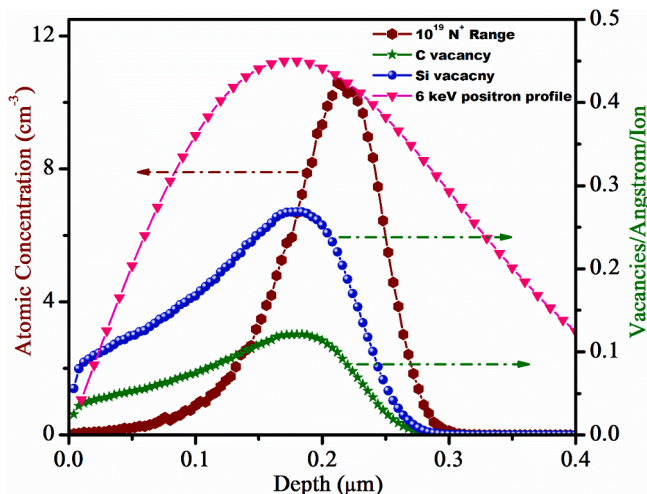
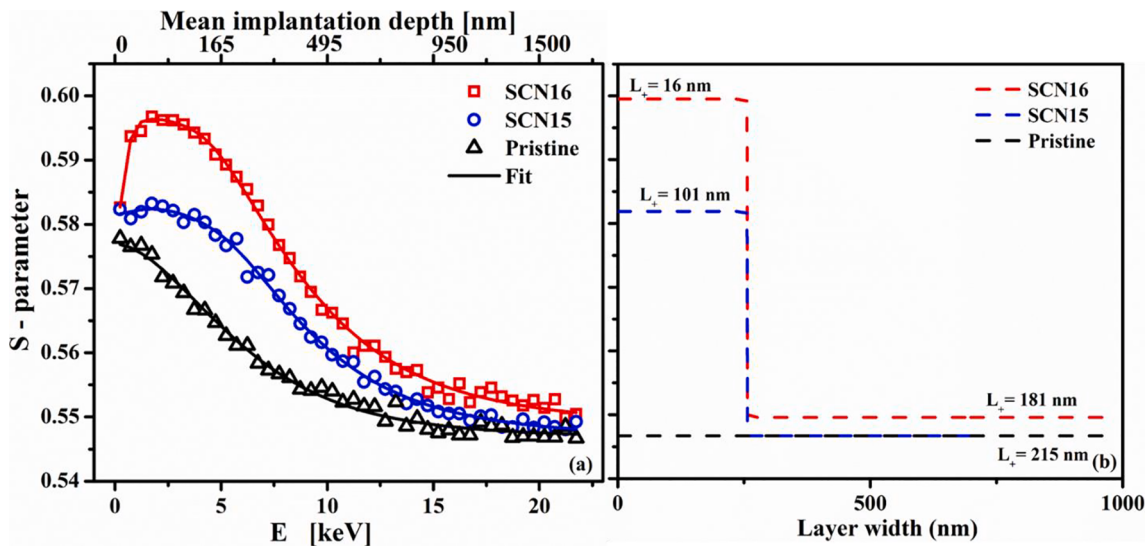


Fig. 1. SRIM evaluated nitrogen concentration, Si vacancy, and C vacancy profile for 130 keV of  $\text{N}^+$  implanted in 6H-SiC with a fluence of  $10^{16} \text{ ions}/\text{cm}^2$  and Makhovian profile for 6 keV incident positron energy.

A single layer VEPFIT model was adopted for the pristine (SCP), considering the homogeneous nature of the sample. The extracted S-bulk value ( $S_b$ )  $0.546 \pm 0.001$  and the positron diffusion length ( $L_{+\text{Ref}}$ ) of  $\sim 215 \pm 6$  nm for pristine is comparable with the reported 200 nm by Barthe et al. [33], 140 nm by Hai-Yun et al. [38] and 160 nm by Kawasuso et al. [39]. Increased  $L_{+\text{Ref}}$  indicate the deep level positron diffusion that annihilated mostly with free electrons, indicating the defect-free nature of pristine. Defect-free pristine sample nature was also reported from the analysis of the characteristic Raman modes [28] and positron DBS measurement [50]. Two homogeneous layers namely damage region (DR) and un-implanted region (UIR) were adopted for the SCN15 sample. The implantation induced damages occurred up to the depth and beyond is due to collision cascade. In the DR layer, implantation created more vacancy concentration thereby reflects a modified electron momentum distribution [18,29]. The fitted average S-parameter and positron diffusion length in this region are  $0.581 \pm 0.002$  and  $101 \pm 34$  nm, respectively. The increase in the average S-value and the reduced diffusion length with that of pristine are associated with the increase in positron trapping at vacancies [10,33,34,51,52]. The obtained DR layer width of  $256 \pm 40$  nm agrees well with the SRIM analysis. Positron diffusion length of  $205 \pm 20$  nm and the average S-parameter of  $0.546 \pm 0.001$  in the UIR are highly comparable with that of pristine.

The implantation damage in SCN16 (High dose sample) showed a considerable S-parameter increase in the near-surface region ( $\sim 70$  nm) and decreased gradually as of SCN15 and SCP. A marginal S-parameter increase in the near-surface in the DR region is an indication of higher damage creation. This confirms the presence of more induced vacancies and vacancy complexes on the near-surface. The S-parameter increases from 0.583 to 0.597 in the positron energy range of 0.235 keV to 1.735 keV. Two layers (DR and UIR) model VEPFIT analysis indicated a positive electric field strength of  $125 \pm 11$  kV/cm in the DR region. Implantation forms many possible types of defects and in-between defects states which include internal induced electric fields. The implantation induced defects electrically modifies the electron motion which acts as a depleted region in the defects states [48]. These induced fields also drift the positrons towards the surface [48]. To understand the presence of electric field strength, the VEPFIT was preceded with and without electric field in DR. Absence of the electric field, resulting in a lower diffusion length (0.5 nm) and an upper layer boundary shift towards the surface (256 nm to 131 nm). These resulted due to the trapping of the positron in defects, similar to the presence of inward-directed electric field as discussed by van Veen et al. [45]. Upon including the electric field ( $125 \pm 11$  kV/cm) for high dose, SCN16 sample resulted in increased DR boundary width  $256 \pm 18$  nm, positron diffusion length  $16 \pm 1$  nm, and S-parameter  $0.599 \pm 0.001$  as tabulated in Table 1. This DR width is highly comparable with the ion depth-profile peak observed from SRIM. The average S-parameter ( $0.549 \pm 0.001$ ) and effective positron diffusion length ( $181 \pm 14$  nm) in the UIR layer is also closer to the pristine value and the small increase in S-value with decreased diffusion length is due to the collision cascade beyond the ion range in high dose sample.

Defects curing and their behaviour were further analyzed using VEPFIT to determine the defect mechanism in the implanted samples annealed at two temperatures in comparison with as-implanted and pristine. Fig. 3(a, c) shows the S(E) of SCN15A8, SCN15A10 and SCN16A8, SCN16A10 compared with pristine and as-implanted. Fig. 3(b, d) displays the depth-dependent VEPFIT derived defect profiles. The electric field strength was also considered for all the annealed samples owing to the layer modifications due activation of charge carriers. The S-parameter for both annealed samples is larger up to a depth of 70 nm due to trapped positrons at the agglomerated defects near the surface and decreased upon annealing indicating the defects recovery in deep. A marginal increase of S-parameter for SCN15A8 ( $0.588 \pm 0.001$ ) in DR can be ascribed to defects agglomeration upon annealing. Moreover, decrease in positron diffusion length ( $17 \pm 3$  nm) and boundary layer



**Fig. 2.** (a) S- parameter as a function of incident positron energy in  $N^+$  implanted 6H- SiC with a fluence of  $10^{15}$  and  $10^{16}$  ions/ $cm^2$  and (b) corresponding S- parameter vs. layer width derived using VEPFIT.

**Table 1**

S- parameter, Positron Diffusion length ( $L$ , nm), and boundary layer ( $B$ , nm) evaluated using VEPFIT for different layers in the ion-implanted and annealed samples. (DR: Damage region, UIR: Unimplanted region). S- Parameter and  $L_{bulk}$  for a pristine sample are,  $0.546 \pm 0.001$  ( $S_b$ ) and  $\sim 215 \pm 6$  nm, respectively. Pristine diffusion length was fixed for SCN15A10 UIR to get a reasonable fit.

Sample	$S_{DR}$	$L_{DR}(\text{nm})$	$B_{DR}(\text{nm})$	Electric field strength (kV/cm)	$S/S_b$ (DR)	$S_{UIR}$	$L_{UIR}$ (nm)
SCN15	$0.581 \pm 0.002$	$101 \pm 34$	$256 \pm 40$	–	1.064	$0.546 \pm 0.001$	$205 \pm 20$
SCN15A8	$0.588 \pm 0.001$	$17 \pm 3$	$221 \pm 22$	$96 \pm 13$	1.077	$0.542 \pm 0.001$	$199 \pm 16$
SCN15A10	$0.589 \pm 0.001$	$16 \pm 2$	$150 \pm 10$	$103 \pm 11$	1.079	$0.542 \pm 0.001$	$215$ (fixed)
SCN16	$0.599 \pm 0.001$	$16 \pm 1$	$256 \pm 18$	$125 \pm 11$	1.097	$0.549 \pm 0.001$	$181 \pm 14$
SCN16A8	$0.581 \pm 0.001$	$68 \pm 39$	$270 \pm 70$	$23 \pm 9$	1.064	$0.547 \pm 0.001$	$216 \pm 26$
SCN16A10	$0.621 \pm 0.001$	$36 \pm 2$	$109 \pm 19$	$124 \pm 22$	1.137	$0.541 \pm 0.001$	$186 \pm 8$

( $221 \pm 22$  nm) with respect to as-implanted  $L_+$  ( $101 \pm 34$  nm) and boundary ( $256 \pm 40$  nm) indicates the defects confinement towards the surface and defects annealing at deep. SCN15A10 fitting leads to a lower diffusion length in UIR ( $120 \pm 19$  nm) with a notable boundary width ( $229 \pm 24$  nm) in DR. This resulted constrains for a best fit and hence, the UIR diffusion length of SCN15A10 was fixed to that of pristine ( $215$  nm). The S- parameter ( $0.589 \pm 0.001$ ) and diffusion length ( $16 \pm 2$  nm) of SCN15A10 deduced from the fit is closer to SCN15A8 with a considerable decrease in boundary width ( $150 \pm 10$  nm). The distinct variation of DR related defect parameters indicates the vacancy agglomeration confined further towards to the surface [18,30,53]. Also, annealing induces the recrystallization in deep as evidenced by the decrease in DR layer boundary width and decrease in UIR layer S- value ( $0.542 \pm 0.001$ ). The observed electric field strength for SCN15A8 and SCN15A10 DR are,  $96 \pm 13$  kV/cm and  $103 \pm 11$  kV/cm, respectively, indicating an inward due to  $N^+$  implantation.

In the case of SCN16A8 samples, adopted with a two-layer model the S- value ( $0.581 \pm 0.001$ ) in DR initially decreases and increases for SCN16A10 ( $0.621 \pm 0.001$ ). Further decrease of S- value ( $0.541 \pm 0.001$ ) in UIR strongly indicates the intrinsic defects recovery. It is seen that positron diffusion length ( $68 \pm 39$  nm) and boundary layer width ( $270 \pm 70$  nm) also increased for the SCN16A8 sample whereas the positron diffusion length ( $36 \pm 2$  nm) and boundary layer width ( $109 \pm 19$  nm) is decreased for SCN16A10. This trend indicates the defect migration and agglomeration towards to surface on the increased annealing temperature. It is significant to note that the observed variations in the DR layer region for  $1000$  °C annealing indicate the formation of larger vacancy clusters at the near-surface with recrystallization in deep. The observed electric field strength for SCN16A8 and SCN16A10 DR are,  $23$  kV/cm and  $124$  kV/cm,

respectively, also towards inward direction due to  $N^+$  implantation.

Fraction of positrons annihilated from the bulk and defect regions vs incident positron energy for all samples is shown in Fig. 4. The sharp changes in the fractions indicates a lower diffusion length and also denotes the significance of electric field. It is well known that the implantations produce more types of inhomogeneous defects distributed in the crystal. Identification of defect types in 6H-SiC is complex due to stacking sequence variation form and its anisotropic behaviour [33]. The decreased DR layer width for  $1000$  °C annealed samples than the  $800$  °C annealed samples confirms the migration of defects towards to surface and aggregated to larger voids [33]. Moreover, Puska *et al.*, [47] and Kuriplach *et al.* [54] reported the low energy positrons may diffuse back after thermalization to the surface in SiC semiconductors.

Studies by optical methods also predominantly displayed divacancies in the damaged region in 6H- SiC [55]. Di-vacancies and vacancy agglomeration with  $N^+/Al^+$  over  $Al^+/N^+$  implanted SiC was also reported [34,51]. Brauer *et al.* reported the presence of di-vacancies in 6H- SiC implanted with  $Ge^+$  at  $200$  keV with higher fluence ( $10^{18}$ – $10^{19}$  ions/ $m^2$ ) and the formation of amorphous layer at the surface [56]. Linez *et al.* [19] theoretically derived the S- values in 6H- SiC and presented well with the experimental studies for various defect types. They have also ascribed the normalized S- values in the range  $1.03$ – $1.07$  to divacancies,  $1.08$ – $1.10$  to unidentified larger defects and  $\sim 1.075$  to trivacancy [19]. The derived S- values  $1.070S_b$  by Linez *et al.* [19] and  $1.068S_b$  by Henry *et al.* [21] in the implanted 6H- SiC was ascribed to  $V_{Si}-V_C$ . Our studies in DR for SCN15 and SCN16 have also resulted to  $1.064S_b$  and  $1.097S_b$ , respectively, indicates the probable presence of divacancies ( $V_{Si}-V_C$ ) and unidentified larger defects [19]. Changes in defect type upon annealing reduce the defects in the deep region and form larger vacancy clusters near the surface [28]. Kuhudzai *et al.*

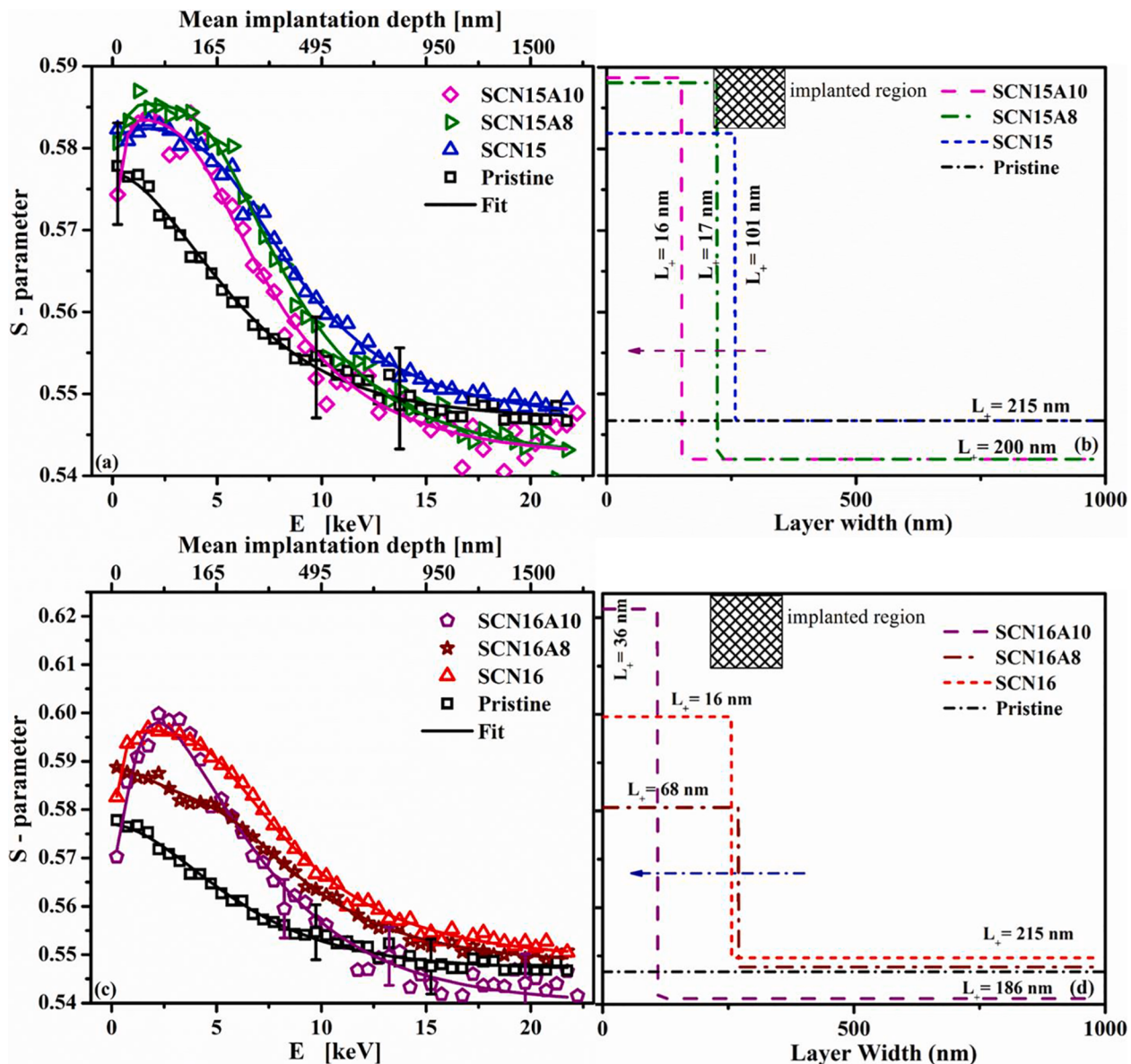


**Fig. 3.** (a),(c)  $S(E)$  profiles of  $\text{N}^+$  implanted and annealed at  $800^\circ\text{C}$  and  $1000^\circ\text{C}$  compared with pristine for the fluence of  $1 \times 10^{15}$  and  $1 \times 10^{16} \text{ N}^+/\text{cm}^2$ , respectively and (b),(d) S- parameter vs. layer width profile derived using VEPFIT.

reported the existence of an amorphous layer in the surface even for  $1200^\circ\text{C}$  annealing [57]. Aboelfotooh and Doyle [58] reported the effect of the annealing from the Si and C vacancy recovery at  $800^\circ\text{C}$  and  $1400^\circ\text{C}$ . Polity *et al.* [59] discussed mixed mono and di- vacancies in electron irradiated and annealed 6H- SiC. Further, Dannefaer and Kerr [60] and Brauer *et al.* [56] reported the presence of vacancy type defects even after annealing to high temperatures. Linez *et al.*, reported the migration of  $V_{\text{Si}}$  combine with  $V_{\text{Si}}\text{-}\text{V}_\text{C}$  thereby forming  $V_{\text{Si}}\text{V}_\text{C}\text{V}_{\text{Si}}$  in  $400^\circ\text{C}$  annealed He implanted 6H- SiC [61]. Comparing the normalized  $S$ - values of SCN15A8 (1.077), SCN15A10 (1.079) and SCN16A8 (1.064) our study indicates the possibility of tri ( $\text{V}_\text{C}\text{V}_{\text{Si}}\text{V}_\text{C}$ ) and di-vacancies, respectively as compared with earlier reports [19,61]. The experimental detector resolution and energy window was also considered to derive the defects types. Hai Yun Wang *et al.* [38] discussed moderate annealing that induces the recombination of vacancies and ion interstitials through implanted ion migration with an effect of the mobility of  $V_{\text{Si}}$  and by forming more ion vacancy complexes. Considerable increase of the normalised  $S$ - value of 1.137 for SCN16A10 indicates the vacancy agglomeration with relaxation of complexes. Electric field

strength induced by the activated charge carriers on annealing was included in the fitting which in turn explored the layer characteristics.

To understand further, the VEPFIT examined  $S$ - parameter, positron diffusion length and boundary width as a function of annealing temperature in DR layer for all the samples presented in Fig. 5 depicts the defect's migration to the surface in the annealed samples. Upon annealing to  $1000^\circ\text{C}$  the defects might have aggregated into larger voids in the surface and induce recrystallization in deep as deduced from the DR layer boundary width that confined towards the surface. In SCN16A8, the diffusion length and boundary width increases with decreasing  $S$ - signifies the diffusion of vacancies and ion- vacancy cluster complexes formation due to high  $\text{N}^+$  concentration. On further annealing, it may be relaxed, to increase the  $S_{\text{DR}}$  and correspondingly decreases the  $L_{\text{DR}}$  and  $B_{\text{DR}}$  exhibits the aggregation of vacancies. Though the present study indicated the possible recrystallization in deep, defects migration towards the surface with the formation of di vacancies and vacancy complexes, further annealing to cure the damaged regions is necessary to complete re-crystallization in deep and dopant activation.

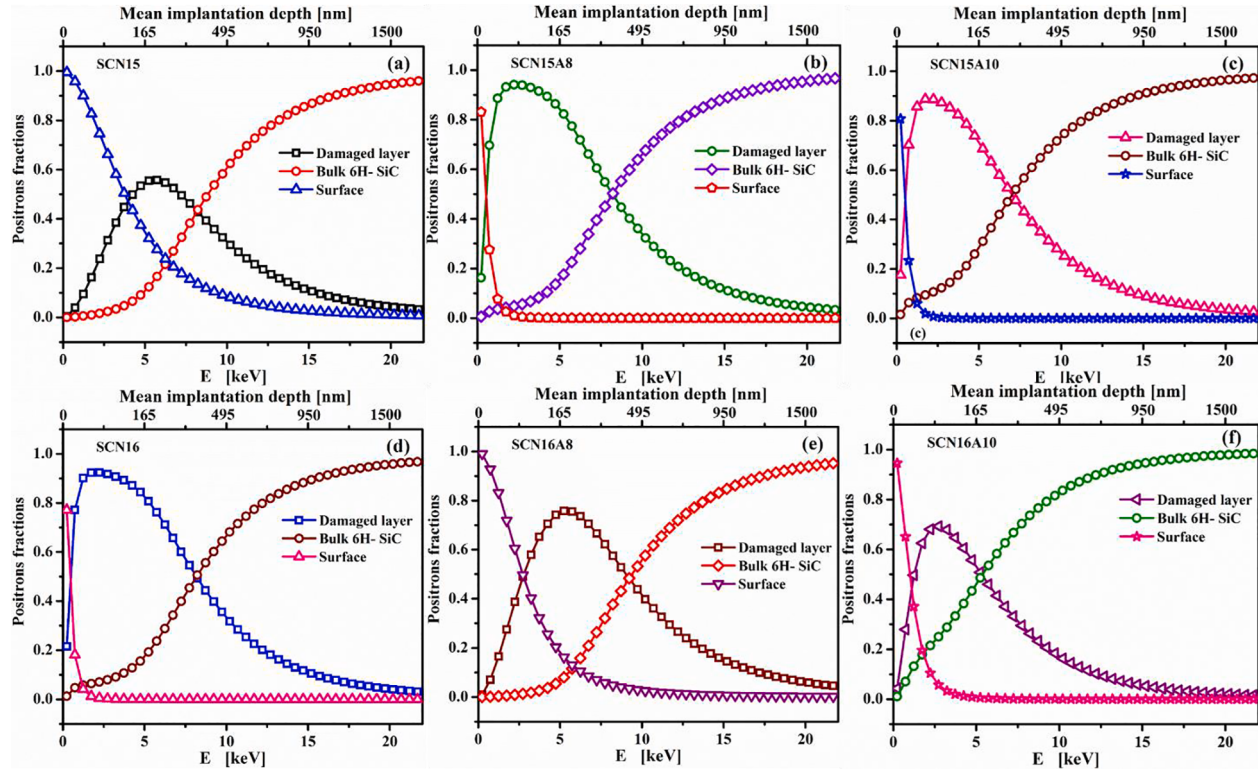


**Fig. 4.** Positron fractions vs energy plots for (a) SCN15, (b) SCN15A8, (c) SCN15A10, (d) SCN16, (e) SCN16A8 and (f) SCN16A10.

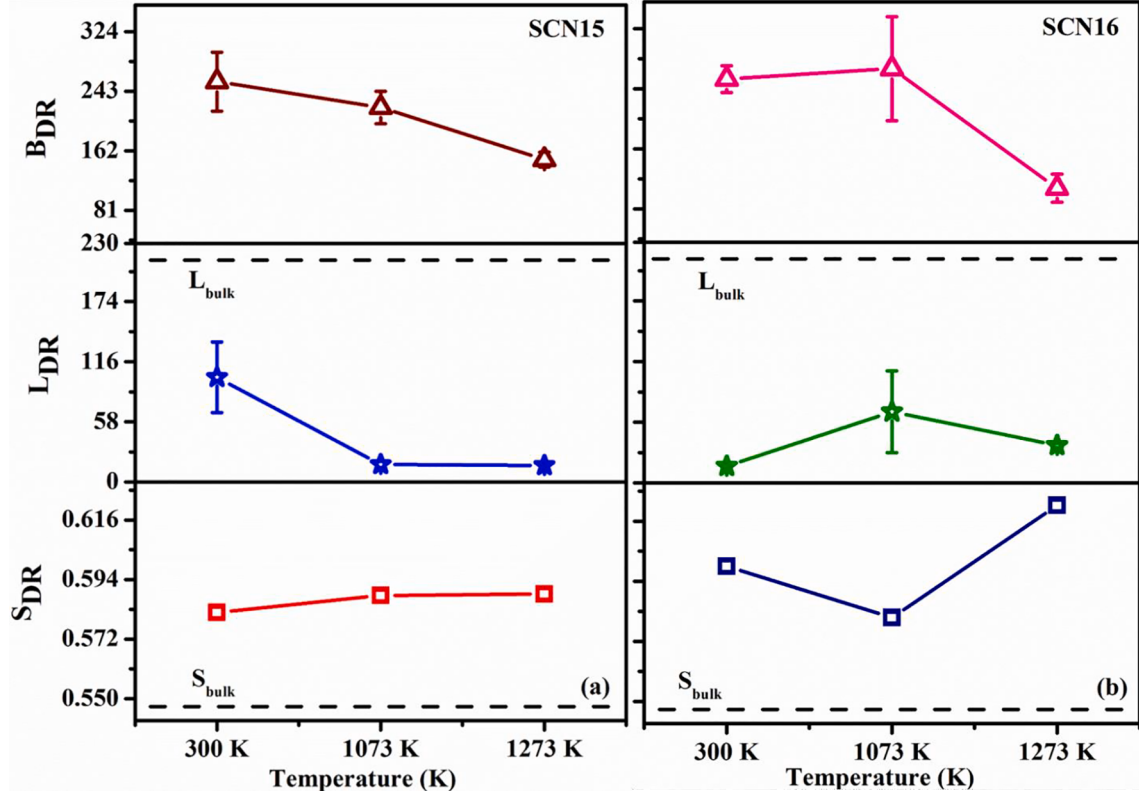


**Fig. 5.** Annealing temperature vs. S-parameter ( $S_{DR}$ ), Positron diffusion length ( $L_{DR}$ ) and Boundary layer width ( $B_{DR}$ ) for SCN15 (a) and SCN16 (b) damage region. 1273 K annealed samples show defects agglomeration in near-surface as evidenced by the decrease of diffusion length, boundary width and increase in  $S_{DR}$ .  $L_+$  value of UIR region was fixed (215 nm) for SCN15A10 during fitting.

#### 4. Conclusion

Selective depth N<sup>+</sup> implantation of two doses at 130 keV in Si- 6H-SiC following the SRIM simulation was achieved with a doping density of 10<sup>19</sup> and 10<sup>20</sup>N<sup>+</sup>/cm<sup>3</sup> at a depth of 200 ± 50 nm. Depth-resolved DBS measurements showed distinct damages at different depths of the implanted regions. Characteristic S variations indicated the electron momentum variations in the damaged regions. Annealing modified the defects with curing and migrations towards the surface. VEPFIT analysis evidenced a distinct S- value reduction together with a variation in positron diffusion length, boundary width, and electric field strength. High-level damage leading to near-surface amorphization, a deep level damage centered at ~ 220 nm indicated the V<sub>Si</sub> increase and correlated well with SRIM analysis. Di-vacancies and vacancy clusters created upon implantation were annealed out in a deep damaged layer and initiated defects migration towards the surface and thereby forming vacancy agglomerations. High-temperature annealing displayed by higher S-parameter near the surface indicated the formation of vacancy clustering due to mobility of defects. Recrystallization and the recovery of deep level defects in 1000 °C annealed sample is evident from the decrease in S- value. The requirement of electric field in fitting methods supported on the activation of charge carriers and evidenced defects signature and region modifications. However, the surface region showed vacancy agglomerations than the most cured damaged region and indicates the need of higher temperature annealing for recrystallized regions.

#### Declaration of Competing Interest

The authors declare that they have no known competing financial interests or personal relationships that could have appeared to influence the work reported in this paper.

#### Acknowledgments

This work was supported by UGC-DAE Consortium for Scientific Research (CSR), Kalpakkam Node, Kokilamedu (Grant No. CSR-KN/CRS-59/2014-15/499 dated 25/08/2014), and measurements were performed at IGCAR, Kalpakkam, and UGC-DAE-CSR. The author KK acknowledges the UGC- DAE-CSR for the award of Junior Research Fellowship and its support.

#### References

- [1] S.E. Saddow, A. Agarwal, *Advances in Silicon Carbide Processing and Applications*, Artech House Inc, Norwood, MA, 2004.
- [2] M. Bhatnagar, B. Jayant Baliga, comparison of 6H-SiC, 3C-SiC, and Si for power devices, *IEEE Trans. Electron Devices* 40 (1993) 645.
- [3] J.W. Palmour, J.A. Edmond, H.S. Kong, C.H. Carter, 6H-Silicon Carbide devices and applications, *Phys. B* 185 (1-4) (1993) 461–465.
- [4] G.A. Slack, Thermal conductivity of pure and impure silicon, silicon carbide, and diamond, *J. Appl. Phys.* 35 (1964) 3460–3466.
- [5] W. v. Muench, I. Pfaffeneder, Breakdown field in vapor-grown silicon carbide p-n junctions, *J. Appl. Phys.* 48 (1977) 4831–4833.
- [6] D. Riedel, F. Fuchs, H. Kraus, S. Väth, A. Sperlich, V. Dyakonov, A.A. Soltamova, P. G. Baranov, V.A. Ilyin, G.V. Astakhov, Resonant addressing and manipulation of silicon vacancy qubits in silicon carbide, *Phys. Rev. Lett.* 109 (2012) 226402.
- [7] W.F. Koehl, B.B. Buckley, F.J. Heremans, G. Calusine, D.D. Awschalom, Room temperature coherent control of defect spin qubits in silicon carbide, *Nature* 479 (2011) 84–87.
- [8] H. Kaneko, T. Kimoto, Formation of a semi-insulating layer in n-type 4H-SiC by electron irradiation, *Appl. Phys. Lett.* 98 (2011) 262106.
- [9] M. Satoh, H. Tanabe, T. Nakamura, Electrical properties of N ion implanted layer in (1100)-oriented 6H-SiC, *Jpn. J. Appl. Phys.* 40 (2001) 114.
- [10] G. Brauer, W. Anwand, W. Skorupa, S. Brandstetter, C. Teichert, Characterization of 6H-SiC surfaces after ion implantation and annealing using positron annihilation spectroscopy and atomic force microscopy, *J. Appl. Phys.* 99 (2006), 023523.
- [11] T. Kimoto, A. Itoh, H. Matsunami, T. Nakata, M. Watanabe, The effects of N+ dose in implantation into 6H-SiC epilayers, *J. Electron. Mater.* 24 (1995) 235–240.
- [12] Y.-T. Yang, R. Han, P. Wang, Raman analysis of defects in n-type 4H-SiC, *Chin. Phys. B* 17 (2008) 3459.
- [13] R. Han, B. Han, D.H. Wang, C. Li, Temperature dependence of Raman scattering from 4H-SiC with hexagonal defects, *Appl. Phys. Lett.* 99 (2011), 011912.
- [14] J. Conrad, T. Riddle, T. Weber, W. Bolse, h-radiation effects in c-SiC studied via RBS-C, Raman-scattering and surface profiling, *Nucl. Instrum. Methods Phys. Res. B* 118 (1996) 748–752.
- [15] D. Dwight, M.V. Rao, O.W. Holland, G. Kelner, P.H. Chi, J. Kretchmer, M. Ghezzo, Nitrogen and aluminum implantation in high resistivity silicon carbide, *J. Appl. Phys.* 82 (1997) 5327–5333.
- [16] M.V. Rao, J.B. Tucker, M.C. Ridgway, O.W. Holland, N. Papanicolaou, J. Mittereder, Ion-implantation in bulk semi-insulating 4H-SiC, *J. Appl. Phys.* 86 (1999) 752–758.
- [17] W.C. Mitchel, R. Perrin, J. Goldstein, A. Saxler, M. Roth, S.R. Smith, J.S. Solomon, A.O. Ewaraye, Fermi level control and deep levels in semi-insulating 4H-SiC, *J. Appl. Phys.* 86 (1999) 5040–5044.
- [18] U. Akira, K. Tomohisa, W. Masahito, M. Tsuyoshi, K. Taka, T. Shiochi, S. Ryoichi, O. Toshiyuki, M. Tomohisa, Effects of recoil-implanted oxygen on depth profiles of defects and annealing processes in P + -implanted Si studied using monoenergetic positron beams, *Jpn. J. Appl. Phys.* 35 (1996) 2000.
- [19] F. Linez, I. Makkonen, F. Tuomisto, Calculation of positron annihilation characteristics of six main defects in 6H-SiC and the possibility to distinguish them experimentally, *Phys. Rev. B* 94 (2016), 014103.
- [20] P.F. Wang, L. Huang, W. Zhu, Y.F. Ruan, Raman scattering of neutron irradiated 6H-SiC, *Solid State Commun.* 152 (2012) 887–890.
- [21] L. Henry, Structure atomique et activité électrique des défauts natifs et induits par irradiation dans le carbone de silicium 6H-SiC déterminées par annihilation de positons, Ph, D thesis, in: Science and Technology, University of Orléans, Orléans, 2002.
- [22] X. Zhang, Q. Li, M. Wang, Z. Zhang, S. Akhmadaliev, S. Zhou, Y. Wu, B. Guo, Defects in hydrogen implanted SiC, *Nucl. Instrum. Methods Phys. Res., Sect. B* 436 (2018) 107–111.
- [23] L. Gordon, A. Janotti, C.G. Van de Walle, Defects as qubits in 3C- and 4H-SiC, *Phys. Rev. B* 92 (2015), 045208.
- [24] F. Fuchs, V.A. Soltamov, S. Väth, P.G. Baranov, E.N. Mokhov, G.V. Astakhov, V. Dyakonov, Silicon carbide light-emitting diode as a prospective room temperature source for single photons, *Sci. Rep.* 3 (2013) 1637.
- [25] E. Morvan, P. Godignon, M. Vellvehi, A. Hallen, M. Linnarsson, A.Y. Kuznetsov, Channeling implantations of Al+ into 6H silicon carbide, *Appl. Phys. Lett.* 74 (1999) 3990–3992.
- [26] G. Brauer, W. Anwand, P.G. Coleman, A.P. Knights, F. Plazaola, Y. Pacaud, W. Skorupa, J. Störmer, P. Willutzki, Positron studies of defects in ion-implanted SiC, *Phys. Rev. B* 54 (1996) 3084–3092.
- [27] C. Varghese Anto, S. Abhaya, P. Magudapathy, G. Amarendra, K.G.M. Nair, Depth profiling of vacancy defects and their thermal stability in N-implanted Si: a positron annihilation study, *J. Phys. D Appl. Phys.* 43 (2010), 325401.
- [28] K. Kamalakkannan, R. Rajaraman, B. Sundaravel, G. Amarendra, K. Sivaji, Effect of nitrogen ion implantation in semi insulating 6H-SiC and recrystallization probed by Raman scattering, *Nucl. Instrum. Methods Phys. Res., Sect. B* 457 (2019) 24–29.
- [29] C.Y. Zhu, C.C. Ling, G. Brauer, W. Anwand, W. Skorupa, Vacancy-type defects in 6H-silicon carbide induced by He-implantation: a positron annihilation spectroscopy approach, *J. Phys. D Appl. Phys.* 41 (2008), 195304.
- [30] P.G. Coleman, R.E. Harding, G. Davies, J. Tan, J. Wong-Leung, The formation, migration, agglomeration and annealing of vacancy-type defects in self-implanted Si, *J. Mater. Sci.: Mater. Electron.* 18 (7) (2007) 695–700.
- [31] M.A. van Huis, A. van Veen, H. Schut, C.V. Falub, S.W.H. Eijt, P.E. Mijnarends, J. Kuripach, Positron confinement in embedded lithium nanoclusters, *Phys. Rev. B* 65 (2002), 085416.
- [32] P.J. Schultz, K.G. Lynn, Interaction of positron beams with surfaces, thin films, and interfaces, *Rev. Mod. Phys.* 60 (1988) 701–779.
- [33] M.F. Barthe, L. Henry, C. Corbel, G. Blondiaux, K. Saarinen, P. Hautojärvi, E. Hugonnard, L. Di Cioccio, F. Letertre, B. Ghyselen, Positron annihilation at proton-induced defects in 6H-SiC/SiC and 6H-SiC/SiO<sub>2</sub>/Si structures, *Phys. Rev. B* 62 (2000) 16638–16644.
- [34] G. Brauer, W. Anwand, P.G. Coleman, W. Skorupa, Slow positron implantation spectroscopy— tool to characterize vacancy-type damage in ion-implanted 6H-SiC, *Vacuum* 78 (2005) 131–136.
- [35] A. Gentils, M.F. Barthe, L. Thomé, M. Behar, Determination of defects in 6H-SiC single crystals irradiated with 20MeV Au ions, *Appl. Surf. Sci.* 255 (2008) 78–80.
- [36] G. Brauer, W. Anwand, P.G. Coleman, J. Störmer, F. Plazaola, J.M. Campillo, Y. Pacaud, W. Skorupa, Post-implantation annealing of SiC studied by slow-positron spectroscopies, *J. Phys. Condens. Matter* 10 (5) (1998) 1147–1156.
- [37] R.S. Yu, M. Maekawa, A. Kawasuso, B.Y. Wang, L. Wei, Positron annihilation study of 4H-SiC by Ge+ implantation and subsequent thermal annealing, *Nucl. Instrum. Methods Phys. Res., Sect. B* 270 (2012) 47–49.
- [38] W. Hai-yun, W. Hui-min, Z. Xian-yl, Defect characterization of 6H-SiC studied by slow positron beam, *Chin. J. Chem. Phys.* 21 (2008) 333.
- [39] A. Kawasuso, F. Redmann, R. Krause-Rehberg, T. Frank, M. Weidner, G. Pensl, P. Sperr, H. Itoh, Vacancies and deep levels in electron-irradiated 6H SiC epilayers studied by positron annihilation and deep level transient spectroscopy, *J. Appl. Phys.* 90 (2001) 3377–3382.
- [40] J.F. Ziegler, M.D. Ziegler, J.P. Biersack, SRIM - The stopping and range of ions in matter (2010), *Nucl. Instrum. Meth. B* 268 (2010) 1818–1823.
- [41] R.S. Brusa, G.P. Karwasz, N. Tiengo, A. Zecca, F. Corni, R. Tonini, G. Ottaviani, Formation of vacancy clusters and cavities in He-implanted silicon studied by slow-positron annihilation spectroscopy, *Phys. Rev. B* 61 (2000) 10154–10166.
- [42] H.S. Krause-Rehberg, Leipner, *Positron Annihilation in Semiconductors: Defect Studies*, Springer-Verlag, Berlin Heidelberg, Heidelberg, 1999.

- [43] J. Dryzek, P. Horodek, GEANT4 simulation of slow positron beam implantation profiles, *Nucl. Instrum. Methods Phys. Res., Sect. B* 266 (2008) 4000–4009.
- [44] A.v. Veen, H. Schut, J.d. Vries, R.A. Hakvoort, M.R. Ijppma, Positron beams for solids and surfaces, *AIP Conf. Proc.* 218 (1990) 171.
- [45] A.v. Veen, H. Schut, J.d. Vries, R.A. Hakvoort, M.R. Ijppma, Analysis of positron profiling data by means of “VEPFIT”, *AIP Conf. Proc.* 218 (1991) 171–198.
- [46] S. Valkealahti, R.M. Nieminen, Monte Carlo calculations of keV electron and positron slowing down in solids. II, *Appl. Phys. A* 35 (1984) 51–59.
- [47] M.J. Puska, P. Lanki, R.M. Nieminen, Positron affinities for elemental metals, *J. Phys. Condens. Matter* 1 (35) (1989) 6081–6094.
- [48] C.C. Ling, H.M. Weng, C.D. Beling, S. Fung, Experimental investigation of slow-positron emission from 4H-SiC and 6H-SiC surfaces, *J. Phys. Condens. Matter* 14 (25) (2002) 6373–6381.
- [49] R. Ramachandran, C. David, P. Magudapathy, R. Rajaraman, R. Govindaraj, G. Amarendra, Study of defect complexes and their evolution with temperature in hydrogen and helium irradiated RAFM steel using positron annihilation spectroscopy, *Fusion Eng. Des.* 142 (2019) 55–62.
- [50] K. Kamalakkannan, C. Lakshmanan, R. Rajaraman, B. Sundaravel, G. Amarendra, K. Sivaji, Positron annihilation studies on Al+ implanted Si-6H-SiC, *AIP Conf. Proc.* 2265 (2020), 030485.
- [51] W. Anwand, G. Brauer, W. Skorupa, Vacancy-type defects in 6H-SiC caused by N+ and Al+ high fluence co-implantation, *Appl. Surf. Sci.* 194 (2002) 131–135.
- [52] V.Y. Bratus, T.T. Petrenko, H.J. von Bardeleben, E.V. Kalinina, A. Hallén, Vacancy-related defects in ion-beam and electron irradiated 6H-SiC, *Appl. Surf. Sci.* 184 (2001) 229–236.
- [53] S.K. Sharma, K. Sudarshan, R. Menon, P.Y. Nabhiraj, P.K. Pujari, He and O ion implantation induced defects in Si crystal studied using slow positron annihilation spectroscopy, *Nucl. Instrum. Methods Phys. Res., Sect. B* 453 (2019) 1–8.
- [54] J. Kuriplach, M. Sob, G. Brauer, W. Anwand, E.M. Nicht, P.G. Coleman, N. Wagner, Positron affinity in semiconductors: Theoretical and experimental studies, *Phys. Rev. B* 59 (1999) 1948–1955.
- [55] W.J. Choyke, The Physics and Chemistry of Carbides, Nitrides and Borides, Vol. 185 of NATO Advanced study institute (Kluwer, Dordrecht, 1990) p.563.
- [56] G. Brauer, W. Anwand, E.M. Nicht, J. Kuriplach, M. Sob, N. Wagner, P.G. Coleman, M.J. Puska, T. Korhonen, Evaluation of some basic positron-related characteristics of SiC, *Phys. Rev. B* 54 (1996) 2512–2517.
- [57] R.J. Kuhudzai, J.B. Malherbe, N.G. van der Berg, T.T. Hlatshwayo, O. Odutemowo, L.C. Prinsloo, A.V. Buys, R. Erasmus, E. Wendler, Deep ultra violet and visible Raman spectroscopy studies of ion implanted 6H-SiC: Recrystallisation behaviour and thermal decomposition/thermal etching of the near surface region, *Nucl. Instrum. Methods Phys. Res., Sect. B* 365 (2015) 342–346.
- [58] M.O. Aboelfotoh, J.P. Doyle, Defect energy levels in electron-irradiated and deuterium-implanted 6H-silicon carbide, *Phys. Rev. B* 59 (1999) 10823–10829.
- [59] A. Polity, S. Huth, M. Lausmann, Defect characterization in electron-irradiated 6H-SiC by positron annihilation, *Phys. Rev. B* 59 (1999) 10603–10606.
- [60] S. Dannefaer, D. Kerr, Positron annihilation investigation of electron irradiation-produced defects in 6H-SiC, *Diam. Relat. Mater.* 13 (2004) 157–165.
- [61] F. Linez, E. Gilabert, A. Debelle, P. Desgardin, M.F. Barthe, Helium interaction with vacancy-type defects created in silicon carbide single crystal, *J. Nucl. Mater.* 436 (2013) 150–157.